Journal of Photochemistry and Photobiology A: Chemistry 207 (2009) 231–235

Contents lists available at ScienceDirect

Journal of Photochemistry and Photobiology A: Chemistry

journal homepage: www.elsevier.com/locate/jphotochem

Defect formation during high-energy ball milling in TiO_2 and its relation to the photocatalytic activity

Roger Amade[a,*], Paul Heitjans[a], Sylvio Indris[a], Mina Finger[b], Andreas Haeger[b], Diethard Hesse[b]

[a] Institut für Physikalische Chemie und Elektrochemie, University of Hannover, Callinstrasse 3-3a, 30167 Hannover, Germany
[b] Institut für Technische Chemie, University of Hannover, Callinstrasse 3, 30167 Hannover, Germany

ARTICLE INFO

Article history:
Received 27 March 2009
Received in revised form 30 June 2009
Accepted 16 July 2009
Available online 24 July 2009

JEL classification:
72.40.+w
81.07.Bc
81.20.wk
82.33.Pt
82.45.Rr
82.50.Hp

Keywords:
Photoconductivity
Photocatalysis
Phase transition
Mechanical attrition

ABSTRACT

High-energy ball milled nanocrystalline TiO_2 (anatase) was analyzed by means of electrochemical impedance spectroscopy in a temperature range from 473 K to 873 K and under reducing and oxidizing atmospheres. The electrical properties are compared with the photocatalytic activity of the samples.

1. Introduction

Titania exists as three main polymorphs: rutile, anatase, and brookite; rutile being the thermodynamically stable one at high temperatures. The anatase structure is particularly known to be the most photocatalytically active one when irradiated with ultraviolet light [1].

Despite its wide use as a photocatalyst some of the catalytic properties of TiO_2 are not well understood. In particular, the temperature dependence of the catalytic activity for the photocatalytic total oxidation of hydrocarbon species in the gas phase suggests that titanium dioxide is reduced and oxidized under reaction conditions (temperature from 298 K to 573 K and atmospheric pressure) [2,3]. At high temperatures the material loses its catalytic activity and becomes coloured, recovering its initial white colour under mild oxidation. Although this fact indicates the formation of defects (colour centres) on the surface of the catalyst [4], most authors interpret the lost of activity as due to coke deposit [5–8] or adsorption processes on the TiO_2 surface [9].

In previous papers [3,10], we discussed the hypothesis that oxygen vacancies are the active sites in the catalytic cycle for photocatalyzed oxidation reaction with TiO_2. Since the defects strongly influence the electrical properties of the material, electrochemical impedance spectroscopy (EIS) [11] can be used to examine this concept. In order to change the defect concentration, mechanical attrition of the catalyst powder by high-energy ball milling [12,13] was performed. Thus, the aim of the present work is to study the influence of the generated defects on the activity (quantum yield) of the catalyst material and on its electrical properties.

Previous works on the surface chemistry of TiO_2 have proposed O atoms/vacancies as the major diffusive species [14–17]. However, a work done by Henderson [18] strongly suggests that titanium interstitials are the major diffusive species in titanium dioxide.

A recent work by Wendt et al. [19] suggests that titanium interstitials in the near-surface region provide the electronic charge needed to enable surface reactions. Our results indicate that titanium interstitials generated by high-energy ball milling are the major diffusive species in titania and are responsible for an increase in its photocatalytic performance, which is in agreement with the works done by Henderson [18] and Wendt et al. [19].

* Corresponding author. Present address: Universitat de Barcelona, Departament de Física Aplicada i Òptica, c/Martí i Franquès 1, 08028 Barcelona, Spain. Tel.: +34 93 403 7089; fax: +34 93 403 9219.
E-mail address: r.amade@ub.edu (R. Amade).

1010-6030/$ – see front matter © 2009 Elsevier B.V. All rights reserved.
doi:10.1016/j.jphotochem.2009.07.015

2. Experimental

Nanocrystalline anatase (Hombifine N, Sachtleben, titanium dioxide 99.99%) with an average grain size of 12 nm was milled in a high-energy ball mill (Spex 8000) for times between 30 min and 4 h. The milling process was done at room temperature in air, with alumina vials and a single alumina ball of 8 mm diameter and a mass of about 4 g. The ball-to-powder weight ratio was 2:1. Abrasion of the grinding tools lead to alumina contamination of the samples between 1.5 and 0.1 weight percentage, depending on the milling time. This amount of alumina is not high enough to significantly change neither the conductivity nor the photocatalytic properties of the samples [11]. X-ray diffraction measurements were performed with a Philips X'Pert MPD system using Cu $K\alpha_1$ radiation ($\lambda = 0.154056$ nm).

2.1. Photocatalysis

The photocatalytic measurements were done by placing the milled powders as a layer in a photoreactor. The residence time distribution of the reactor equates to a continuous stirred tank reactor. The layer of catalyst is irradiated from a light source above the reactor. A detailed description of the photoreactor and experimental setup used for photocatalytic measurements can be found elsewhere [20].

The absorption coefficient of the catalyst material was determined by means of diffuse reflectance spectroscopy using a spectrophotometer DMC 25 (Carl Zeiss, Oberkochen). It was assured that the thickness of the catalyst probes was sufficient to avoid the transmission of light, therefore the absorption coefficient $\alpha(\lambda)$ could be calculated from the diffuse remission coefficient $\beta(\lambda)$, see Eq. (1):

$$\alpha(\lambda) = 1 - \beta(\lambda) \tag{1}$$

The spectrum of the lamp $I_0(\lambda)$ (Philips HPA 1000/20) was determined using a photodiodearrayspectrometer (Dr. Gröbel UV-Elektronik, Ettlingen). The spectrum of the light absorbed from the catalyst plate, $I_a(\lambda)$ [W/(m^2 nm)], was calculated by multiplying the values of $\alpha(\lambda)$ with $I_0(\lambda)$, see Fig. 1.

With the energy of a photon, $E_{Phot} = h\nu$, wherein ν denotes the frequency and h Planck's constant, the moles of photons absorbed per second and geometric surface area of the catalyst sample, I_P^* [mol/(s m^2)], is calculated according to Eq. (2). N_A denotes the Avogadro constant.

$$I_P^* = \frac{1}{N_A}\int_{\lambda=300\,\mathrm{nm}}^{\lambda=420\,\mathrm{nm}} \frac{I_a(\lambda)}{E_{Phot}(\lambda)}d\lambda \quad [\mathrm{mol/(s\ m^2)}] \tag{2}$$

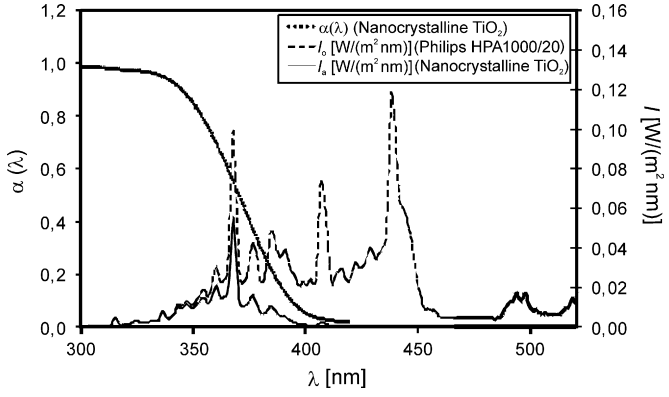

Fig. 1. Spectrum of the lamp $I_0(\lambda)$, absorption coefficient of the catalyst material $\alpha(\lambda)$ using nanocrystalline anatase (Hombifine N, Sachtleben, Duisburg) as an example and spectrum of the light absorbed by the catalyst sample $I_a(\lambda)$.

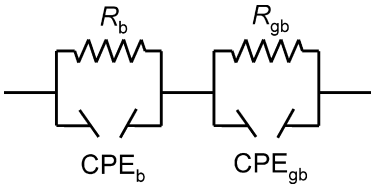

Fig. 2. Equivalent circuit used to describe the electrical response of the samples. R_b and CPE_b are the resistance and the constant phase element ascribed to the bulk, and R_{gb} and CPE_{gb} are the resistance and the constant phase element ascribed to the grain boundaries.

The quantum yield regarding to a reactant i, Q_i [%], which was defined as the ratio of reaction rate and absorption rate of photons of the catalyst sample is given by Eq. (3),

$$Q = \frac{r_A}{I_P^*} \times 100 \tag{3}$$

wherein r_A [mol/(s m^2)] denotes the reaction rate per geometric surface area under steady state conditions.

2.2. Impedance spectroscopy

The samples for impedance spectroscopy were prepared by conventional room temperature compression at 1 GPa. With this method pellets with a diameter of 8 mm and a thickness between 0.5 mm and 2 mm were obtained. The electrodes were prepared by physical vapour deposition (PVD) of gold.

The impedance of the samples was measured with a HP 4192 A impedance analyzer. An alternating voltage of 100 mV was applied in a frequency range from 5 Hz to 13 MHz. The samples were measured in oxygen atmosphere ($PO_2 = 10^5$ Pa) and vacuum ($PO_2 = 10^2$ Pa), and in a temperature range from room temperature up to 973 K.

The impedance spectra were fitted with a non-linear least squares fit (NLLSF) program (equivalent circuit [21]). Two overlapping semicircles were observed for most of the samples. Since the fastest polarization processes take place in the bulk [11], it was assumed that the high-frequency arc corresponds to this part of the material and the low frequency arc to the grain boundaries. The equivalent circuit used to describe the electrical response of the samples is shown in Fig. 2. R_b, R_{gb} are the resistances, and CPE_b, CPE_{gb} are the constant phase elements (CPE) ascribed to the bulk and the grain boundaries, respectively. Ideally, one should be able to represent a material with a resistance R and a capacitance C in parallel, which corresponds to a single relaxation time. However, due to the non-ideality of the real world, the CPE is commonly used to describe a system which due to inherent inhomogeneities cannot be described by a simple RC circuit. The CPE is used when the semicircles are depressed, which indicates a distribution of relaxation times [11].

The conductivities of the bulk and the grain boundaries can be easily calculated from the results of the fitting process and the dimensions of the samples. However, the conductivity calculated in such a way is actually a volume-extensive conductivity [11], which means that it depends on the conductivity of the bulk and the grain boundaries, but *also* on the respective volume fraction in the sample. Since we do not know the volume fractions of the two regions (bulk and grain boundaries) we will use the term conductivity to refer to the volume-extensive conductivity of each region.

From the temperature dependence of the conductivity the activation energy of the conduction process was calculated using the Arrhenius equation [22]:

$$\sigma_{\mathrm{dc},i}T = A_i \exp\left(\frac{-E_{A,i}}{kT}\right) \tag{4}$$

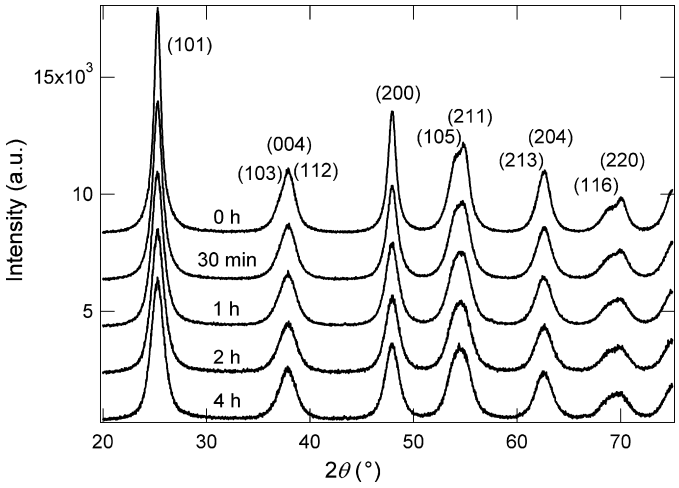

Fig. 3. XRD pattern of nanocrystalline anatase milled up to 4 h. Neither the formation of a new phase nor a broadening of the lines with milling can be recognised. The slight decrease of the peak intensities with milling indicates the formation of amorphous regions in the material.

where $\sigma_{dc,i}$ is the direct current (dc) conductivity of region i (i = bulk or grain boundaries), calculated from the fitting parameters and the dimensions of the sample. A_i is the pre-exponential factor of region i, and $E_{A,i}$ is the activation energy in region i. T is the temperature and k is the Boltzmann constant.

Further information can be extracted from the real part of the ac (alternate current) conductivity, which may be expressed by the power law [11,23,24].

$$\sigma_i' = \sigma_{dc,i} + A_{p,i}\omega^{n_i} \quad (5)$$

where σ_i' is the real part of the conductivity, $\sigma_{dc,i}$ has the same meaning as in equation 4, $A_{p,i}$ is a prefactor and n_i an exponent with $0 < n_i < 1$.

Different values of n have been observed for different kinds of materials. In systems with carrier transport (e.g., electronic hopping, movement of ions) [21] n takes values in the range $0.5 < n < 0.9$. For polymers and glasses above the glass transition temperature values of about 0.4 have been reported [25–27].

3. Results

Fig. 3 shows the XRD patterns of the milled nanocrystalline samples. The average crystallite size could be obtained via the Scherrer equation:

$$L_0 = \frac{K\lambda}{\beta \cos\theta} \quad (6)$$

where K = Scherrer constant, λ = X-ray wavelength, β = width of the XRD peak after corrections concerning instrumental broadening and θ = diffraction angle. A constant particle size of about 10 nm was obtained from the breadth of the peaks. Neither big changes in the width and height of the lines nor the formation of new phases can be recognised during milling. The influence of lattice imperfections (strain) on the line breadth is dominant in materials with large crystallite sizes. For fine powders (crystallite sizes below 100 nm), the line broadening is mainly dominated by the small grain sizes rather than by the strain. The slight decrease in the intensity of the lines with milling time indicates the formation of some amorphous phase.

A surface area of about 200 $m^2\,g^{-1}$ is obtained for all samples from BET-surface area measurements [28] which agrees with the XRD results.

In a previous article [20] we reported on the characterization of milled microcrystalline titania and found that the concentration of Ti^{3+} interstitials increases with milling time. In the present work the grain size of the milled nanocrystalline samples remained constant with milling time, and therefore we expect that, since the mechanical energy is not used to decrease the crystallite size, it is used to generate more defects during the milling process.

3.1. Photocatalysis

The following reaction was used to analyze the photocatalytic activity of TiO_2:

$$C_3H_6 + (9/2)O_2 \rightarrow 3CO_2 + 3H_2O \quad (7)$$

Fig. 4 shows the quantum yield of nanocrystalline anatase for the total oxidation of propene at different oxygen partial pressures versus milling time. A maximum is observed at around 45 min depending on the partial pressure. Since the particle size remained constant for all milling times (~12 nm) and the catalytic processes take place near the surface of the catalyst, the maximum can be attributed to the generation of defects in this region.

3.2. Impedance spectroscopy

The activation energy in each region is independent of its volume fraction in the sample, and therefore we can compare their values. On the contrary, the dc conductivity depends on the volume fraction of the region and therefore, we cannot compare the conductivities of the grain boundaries and the bulk. However, we can assume that the volume fraction of grain boundaries remains more or less constant because the grain size does not change and the density of the samples remained constant with milling time. In that case, we can compare the conductivity of one of the two regions after a certain milling time with the conductivity of the *same* region at a different milling time, but not with a different region.

Fig. 5 shows a typical impedance spectrum with two overlapping semicircles. The inset shows an Arrhenius plot of the bulk and grain boundary regions. The arrow indicates the point obtained by fitting the impedance spectrum with the equivalent circuit shown in Fig. 2.

Due to the low temperatures of the measurements and due to the high overlap of the semicircles, the activation energies of the

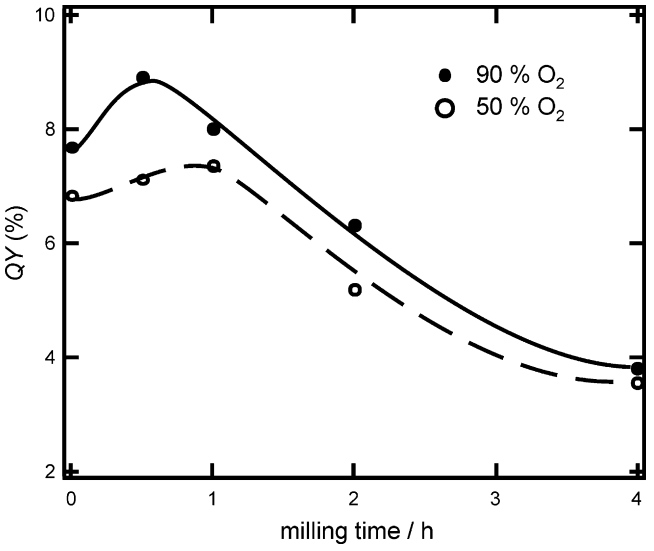

Fig. 4. Quantum yield of milled nanocrystalline anatase for the total oxidation of propene at different oxygen partial pressures versus milling time [29]. The solid and dashed lines are drawn to guide the eye.

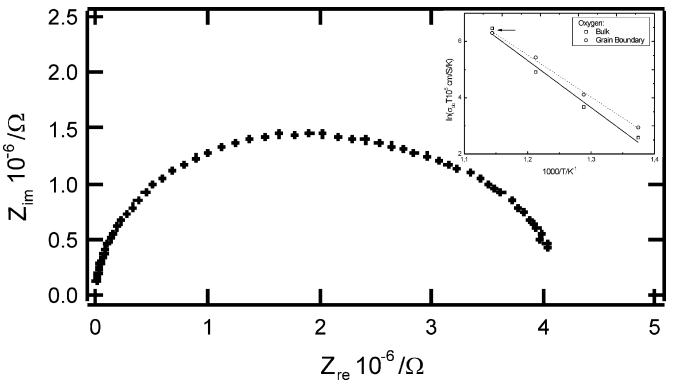

Fig. 5. Impedance spectrum of nanocrystalline anatase milled for 1 h, measured at 873 K in oxygen atmosphere. The inset shows an Arrhenius plot of the bulk and grain boundary regions. The arrow indicates the point obtained by fitting the impedance spectrum with the equivalent circuit shown in Fig. 2.

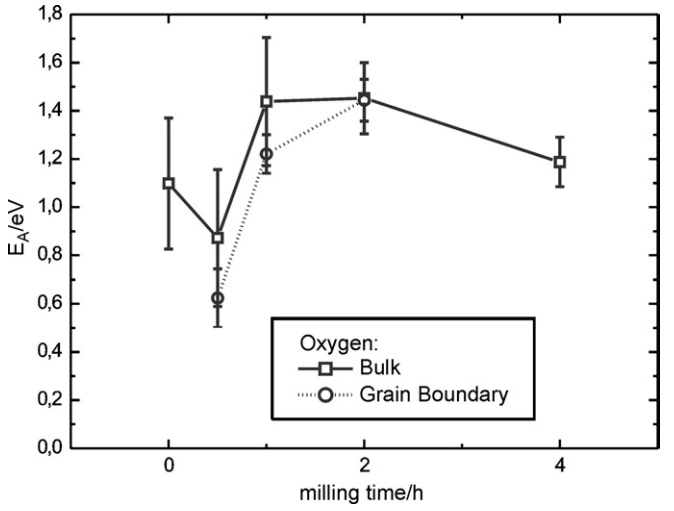

Fig. 6. Activation energies in oxygen atmosphere of the bulk and grain boundaries of nanocrystalline anatase milled for different milling times.

conduction process in the grain boundaries and in the bulk have large error bars.

Figs. 6 and 7 show these activation energies found for the milled nanocrystalline samples in oxygen atmosphere and in vacuum,

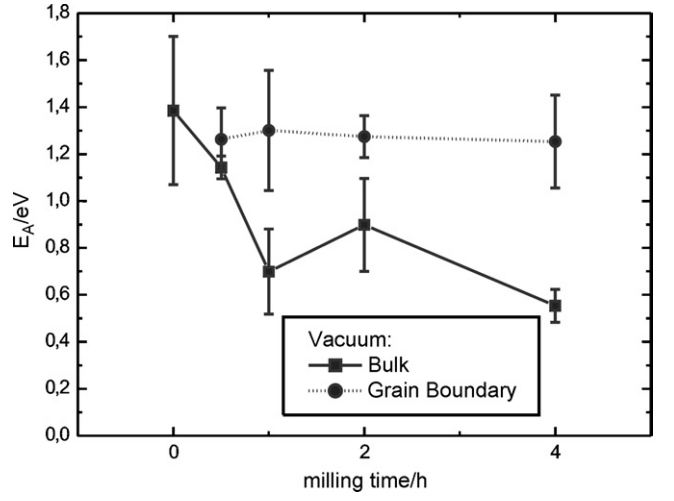

Fig. 7. Activation energies in vacuum of the bulk and grain boundaries of nanocrystalline anatase milled for different milling times.

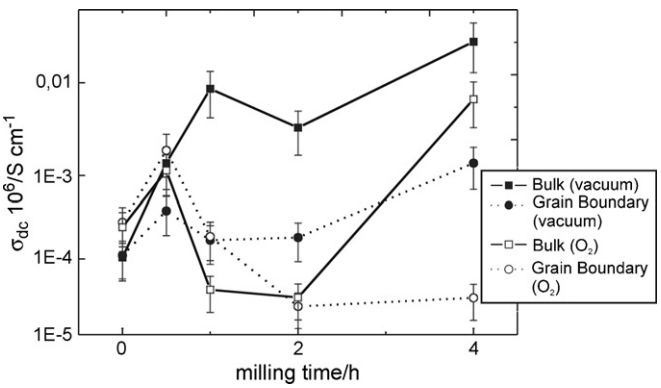

Fig. 8. Variation of the dc conductivity with the milling time at $T = 573$ K and at $PO_2 = 10^5$ Pa (open symbols) and $PO_2 = 10^2$ Pa (full symbols).

respectively. Some points for the grain boundary region are missing, this is due to the high overlapping of the semicircles. In some cases they could not be separated and therefore the Arrhenius plots had a too small number of points from which the activation energy could not be calculated.

The results show a minimum in the activation energies at a milling time of about 30 min for the measurements performed in oxygen atmosphere. This value corresponds well with the milling time where the maximum in the photocatalytic activity measurements was found.

For the measurements performed in vacuum, the activation energy of the grain boundary remains more or less constant around 1.3 eV, while that of the bulk decreases, starting at 1.3 eV, down to about 0.6 eV.

Fig. 8 shows the dc conductivities of the bulk and the grain boundaries in the two different atmospheres at 573 K. Although the error bars are large, the differences between the conductivities are large enough to consider the maximum at around 45 min milling time as being reliable. Such a maximum in the conductivity can only be explained by a change in the conduction mechanism or in the structure of the grains. The values of n were found to be between 0.5 and 0.9, which indicates electron hopping or movement of ions [24] (see Eq. (5)).

4. Discussion

Both the photocatalytic and impedance measurements show a change of behaviour after a milling time of about 45 min. While the quantum yield and the dc conductivity pass through a maximum at this point, the activation energy in oxygen atmosphere reveals a minimum around 0.6 eV. This value is close to the one found by Hoshino et al. [29] (0.7 eV) for the diffusion of Ti^{3+} and Ti^{4+} interstitials. The presence of Ti^{3+} was found to increase with milling time and was reported in another paper by us [20]. For long milling times the activation energy is close to 1.4 eV. The reduction reaction

$$Ti_{Ti} + O_O \rightarrow Ti'_{Ti} + V_O^{\cdot\cdot} + e' + \tfrac{1}{2}O_2 \quad (8)$$

was found to have an activation energy of 1.42 eV in a nanocrystalline anatase sample [30], where Ti'_{Ti} corresponds to a Ti^{3+} ion in a titanium site, $V_O^{\cdot\cdot}$ to a doubly ionized oxygen vacancy and the other symbols have the usual meaning.

Therefore, for long milling times a reduction of the sample might occur, while at shorter milling times the conduction of ions (titanium interstitials) prevails. These results indicate a relation between a highly defective structure with ionic conductivity and a high photocatalytic activity. Consequently, the increase in the dc conductivity can be ascribed to an increase of the defect concentration, which allows a faster movement of the ions (Ti^{3+} interstitials).

At milling times longer than about 45 min these defects may coalesce [31] and form a new phase [32] with a lower conductivity in the grain boundaries and a lower photocatalytic activity. This supposed new phase was not observed from XRD measurements. However, it is possible that this phase consists of a thin layer in the near-surface region of the grains and is therefore not seen with XRD. At long milling times, a reduction of the bulk takes place in oxygen atmosphere, which does not increase the photocatalytic activity of the material, in accordance with the relation between ionic conduction and catalytic activity mentioned above. Therefore, at long milling times there is a further reduction of the material that increases the electronic conductivity and reduces the ionic conductivity. This effect is bigger in vacuum atmosphere than in oxygen and it reduces the photocatalytic activity of the material.

For that reason, the maximum found in the temperature dependence of the photocatalytic activity [4] (see Section 1) is likely related to a high content of defects (oxygen vacancies and titanium interstitials) in the catalyst, and the decrease of the catalytic activity at high temperatures is probably related to an excessive reduction of the bulk, rather than to adsorption processes or coke deposit.

In vacuum the activation energy of the grain boundaries is about 1.3 eV for all milling times, suggesting that the material has a different conduction mechanism from that in oxygen atmosphere and is already reduced at short milling times. On these conditions no ionic conduction takes place at the grain boundaries, and therefore, we would expect lower catalytic activity than in oxygen, as corroborated by the results shown here.

5. Conclusions

Impedance measurements on milled nanocrystalline titanium dioxide samples have been used to characterize the electrical properties of the material in the grain boundaries and bulk regions. It has been shown, that the defects formed during the milling process alter the conductivity and the photocatalytic activity of the samples, and play an important role during the catalytic processes. A higher number of defects, mainly Ti^{3+} interstitials, and a high ionic mobility has been related to a higher photocatalytic activity. We propose that at a certain defect concentration (or after about 45 min of milling time) a phase transition takes place in the catalyst leading to a reduction of the material and to a loss of its catalytical properties.

Acknowledgement

We are grateful to the Deutsche Forschungsgemeinschaft (DFG) for financial support.

References

[1] A.L. Linsebigler, G. Lu, J.T. Yates Jr., Photocatalysis on TiO_2 surfaces: principles, mechanisms, and selected results, Chem. Rev. 95 (1995) 735–758.
[2] A. Haeger, O. Kleinschmidt, D. Hesse, Kinetics of photocatalyzed gas reactions using titanium dioxide as the catalyst. Part I: Photocatalyzed total oxidation of olefines with oxygen, Chem. Eng. Technol. 27 (2004) 181–188.
[3] A. Haeger, O. Kleinschmidt, D. Hesse, Kinetics of photocatalyzed gas reactions using titanium dioxide as the catalyst. Part II: Photocatalyzed total oxidation of alkanes with oxygen, Chem. Eng. Technol. 27 (2004) 1019–1026.
[4] R. Amade, P. Heitjans, S. Indris, M. Finger, A. Haeger, D. Hesse, Influence of gas atmosphere and temperature on the conductivity of TiO_2 single crystal in the surface region, Phys. Chem. Chem. Phys. 8 (2006) 777–782.
[5] Y. Luo, D.F. Ollis, Heterogeneous photocatalytic oxidation of trichloroethylene and toluene mixtures in air: kinetic promotion and inhibition, time-dependent catalyst activity, J. Catal. 163 (1996) 1–11.
[6] L. Cao, Z. Gao, S.L. Suib, T.N. Obee, S.O. Hay, J.D. Freihaut, Photocatalytic oxidation of toluene on nanoscale TiO_2 catalysts: studies of deactivation and regeneration, J. Catal. 196 (2000) 253–261.
[7] S. Sitkiewitz, A. Heller, Photocatalytic oxidation of benzene and stearic acid on sol–gel derived TiO_2 thin films attached to glass, New J. Chem. 20 (1996) 233–241.
[8] A.V. Vorontsov, E.N. Kurkin, E.N. Savinov, Study of TiO_2 deactivation during gaseous acetone photocatalytic oxidation, J. Catal. 186 (1999) 318–324.
[9] J.-M. Herrmann, Active agents in heterogeneous photocatalysis: atomic oxygen species vs. OH radicals: related quantum yields, Helv. Chim. Acta 84 (2001) 2731–2750.
[10] M. Finger, A. Haeger, D. Hesse, Kinetics and mechanisms of photocatalyzed total oxidation reaction of hydrocarbon species with titanium dioxide in the gas phase, Chem. Eng. Technol. 28 (2005) 783–789.
[11] E. Barsoukov, J.R. Macdonald (Eds.), Impedance Spectroscopy: Theory, Experiment, and Applications, second ed., John Wiley Sons, New York, 2005.
[12] S. Indris, D. Bork, P. Heitjans, Nanocrystalline oxide ceramics prepared by high-energy ball milling, J. Mater. Synth. Process. 8 (2000) 245–250.
[13] P. Heitjans, S. Indris, Fast diffusion in nanocrystalline ceramics prepared by ball milling, J. Mater. Sci. 39 (2004) 5091–5096.
[14] V.E. Henrich, G. Dresselhaus, H.J. Zeiger, Observation of 2-dimensional phases associated with defect states on surface of TiO_2, Phys. Rev. Lett. 36 (1976) 1335–1339.
[15] W.J. Lo, Y.W. Chung, G.A. Somorjai, Electron-spectroscopy studies of chemisorption of O_2, H_2 and H_2O on TiO_2(1 0 0) surfaces with varied stoichiometry—evidence for photogeneration of Ti^{3+} and for its importance in chemisorption, Surf. Sci. 71 (1978) 199–219.
[16] W. Göpel, G. Rocker, R. Feierabend, Intrinsic defects of TiO_2(11 0)—interaction with chemisorbed O_2, H_2, CO and CO_2, Phys. Rev. B 28 (1983) 3427–3438.
[17] J.T. Mayer, U. Diebold, T.E. Madey, E. Garfunkel, Titanium and reduced titania overlayers on titanium dioxide (1 1 0), J. Electron Spectrosc. Relat. Phenom. 73 (1995) 1–11.
[18] M.A. Henderson, A surface perspective on self-diffusion in rutile TiO_2, Surf. Sci. 419 (1999) 174–187.
[19] S. Wendt, et al., The role of interstitial sites in the Ti3d defect state in the band gap of titania, Science 320 (2008) 1755–1759.
[20] S. Indris, R. Amade, P. Heitjans, M. Finger, A. Haeger, D. Hesse, W. Grünert, A. Börger, K.D. Becker, Preparation by high-energy milling, characterization, and catalytic properties of nanocrystalline TiO_2, J. Phys. Chem. B 109 (2005) 23274–23278.
[21] B.A. Boukamp, A package for impedance admittance data-analysis, Solid State Ionics 18–19 (1996) 136–140.
[22] A.R. West, Basic Solid State Chemistry, John Wiley Sons, Chichester, 1987.
[23] A.K. Jonscher, Universal Relaxation Law, second ed., Chelsea Dielectrics Press, London, 1996.
[24] A.K. Jonscher, Universal dielectric response, Nature 267 (1977) 673–679.
[25] K.L. Ngai, A.K. Jonscher, C.T. White, Origin of the universal dielectric response in condensed matter, Nature 277 (1979) 185–189.
[26] K.L. Ngai, A review of critical experimental facts in electrical relaxation and ionic diffusion in ionically conducting glasses and melts, J. Non-Cryst. Solids 203 (1996) 232–245.
[27] C.A. Angell, Dynamic processes in ionic glasses, Chem. Rev. 90 (1990) 523–542.
[28] M. Finger, Diploma Thesis, University of Hannover, 2003.
[29] K. Hoshino, N.L. Peterson, C.L. Wiley, Diffusion and point-defects in TiO_{2-x}, J. Phys. Chem. Solids 46 (1985) 1397–1411.
[30] D. Eder, R. Kramer, Stoichiometry of "titanium suboxide"—Part 2. Electric properties, Phys. Chem. Chem. Phys. 5 (2003) 1314–1319.
[31] L.A. Bursill, D.J. Smith, Interaction of small and extended defects in nonstoichiometric oxides, Nature 309 (1984) 319–321.
[32] T. Girot, S. Bégin-Colin, X. Devaux, G. Le Caër, A. Mocellin, Modeling of the phase transformation induced by ball milling in anatase TiO_2, J. Mater. Synth. Process. 8 (2000) 139–144.